Design, fabrication and characterisation of Si-based capillary-driven microfluidic devices

Yifei Ye[1,2], *Yang Zhao*[1], *Jie Cheng*[1,2], *Mingxiao Li*[1], *Chengjun Huang*[1,2] ✉

[1]*R&D Center of Healthcare Electronics, Institute of Microelectronics, Chinese Academy of Sciences, Beijing 100029, People's Republic of China*
[2]*School of Future Technology, University of Chinese Academy of Sciences, Beijing 100049, People's Republic of China*
✉ *E-mail: huangchengjun@ime.ac.cn*

Published in Micro & Nano Letters; Received on 21st March 2018; Revised on 4th May 2018; Accepted on 10th August 2018

Capillary-driven microfluidic devices have a great potential for the point-of-care testing systems based on the advantages of self-pumping, low reagent usage and rapid detection. Here, the study presents a lidless Si-based capillary-driven microfluidic device, comprising two inlets for sample and buffer loading, a snake-shaped microchannel (120/0.05/0.025 mm in length/width/depth) as a flow resistor, a micropillar array (25/5/8 μm in height/diameter/pitch) as a capillary pump and a vent. It was fabricated with lithographic technique in combination with deep Si etch technique. A simple and stable surface hydrophilisation modification method was demonstrated on the device by forming a self-assembly monolayer through Cu-catalysed azide-alkyne cycloaddition reaction. The surface modified device allowed controllable autonomous capillary flow delivery with a contact angle of around 40° stabilised for at least 90 days. The design of two inlets with one common long snake-shaped microchannel provided the sequential capillary flow generation and propagation with controlled flow rate and propagation distance, while the micropillar array with a high aspect ratio of 5 was considered as an effective capillary pump. Based on the obtained results, the proposed device makes possible for the on-chip biosensing applications as a part of integrated point-of-care testing systems.

1. Introduction: Implementing complex bioanalytical assays on fully integrated and scalable lab-on-a-chip devices has a great potential in key biomedical applications such as point-of-care testing (POCT) [1]. The microfluidic system is attracting extensive attention as it provides many advantages, such as high sensitivity, fast reaction, low sample and time consumption [2]. In the conventional microfluidic systems, various microfluidic handlings of liquid samples, e.g. pumping, stopping, mixing, washing, are required for the different purpose [3, 4]. A number of methods have been proposed for such microfluidic actuations, in which various driving mechanisms, such as electric, magnetic, mechanical and optical ones, have been utilised. However, these methods for microfluidic actuations generally include external control units, such as pumps, valves and macro to microfluidic interfaces [1, 2]. These units dramatically increase the complexity and cost of the microfluidic system, as well as the challenges for further miniaturisation. Compared with the 'active' microfluidic systems, the capillary-driven microfluidic devices (CMDs) have received increasing interests as they drive the liquid sample by the natural capillary forces and do not require any active components, thus especially suitable for POCT applications [5–7]. By virtue of the abundance and physical properties of the materials, the paper-based strips have been successfully used on various POCT applications, such as the strips for pregnancy test and glucose test of diabetes [8, 9]. The liquid movements inside these strips are controlled by the wet capability and the feature size of the porous strips which are usually made of cellulose, nitrocellulose or other polymer films [9]. Although these devices are simple, cheap and easy to use, this type of lateral flow devices usually only allow unidirectional sample movement and mixing, and has a relatively large dead volume as the entire strip must be filled to drive the capillary flow. These drawbacks make the paper strips difficult to perform exact and complex fluidic handlings, thus not suitable for complex bioassay detection [9, 10]. It is necessary to find a technique to realise controlled capillary flow, which may be especially valuable for the complex and multi-step biological assay in POCT applications.

Recently, researchers demonstrated the opportunities on Si and plastic-based devices to achieve various liquid handlings, such as unidirectional, anisotropic and multilayer spreading by using three-dimensional microstructures, and successfully applied these devices for complex immunoassays [9, 11–14]. For example, the different-size microchannels can be used for autonomous flow propagation, stopping and mixing without any valves [13, 15]. Lillehoj *et al.* [13] integrated an electrochemical sensor on a self-pumping capillary device comprising several long snake-shaped microchannels for detecting botulinum toxin. However, the capillary capability generated by these microchannels is still relatively low. Compared to the microchannel for capillary flow generation, the micropillar array has better capillary ability and lower clogging probability as it has much higher hydrophilic surface area per unit length, and smaller effective pore diameter [16, 17]. Jonsson *et al.* [11] used a polymer-based '4castchip' with micropillar array as a replacement of the paper strip, and developed a sandwich immunoassay for detecting C-reactive protein. However, due to the design and structural limit of the device, it is only suitable for the application of one directional capillary flow and relatively simple assay. In order to have a more flexible control of the capillary flow, researchers combined the microchannel as a flow resistor and the micropillar array as a capillary pump [18], i.e. Novo *et al.* [14] designed a CMD with four different inlets and achieved sequential fluid flow for multi-step immunoassays; Gervais and Delamarche [12] demonstrated a Si-polydimethylsiloxane hybrid CMD consisting of a microchannel and a micropillar array for multi-parametric immunoassays. However, these reported devices still have limitations, such as low capillary capability, high risk of clogging and air bubble generation.

In this study, we proposed a new lidless Si-based CMD, which integrated the microchannels, a T junction and micropillar array into a single chip. After the surface hydrophilisation modification by forming a self-assembly monolayer (SAM) through Cu-catalysed azide-alkyne cycloaddition reaction, a contact angle of around 40° was stabilised for at least 90 days [1, 19, 20]. The proposed device allowed autonomous sequential flow propagation with

doi: 10.1049/mnl.2018.5120

controllable flow rate while without the need of valves or any external actuation. Comparing to the reported capillary flow devices, our device has the advantages of easy fabrication, straightforward cleaning and low risk of clogging and generation of air bubbles [12, 16, 21]. The obtained results showed that the proposed Si-based capillary microfluidic device has a great potential for the multi-step bioassays in POCT applications.

2. Methods and experimental

2.1. Device design: The lidless CMD consists of a sample inlet, a buffer inlet, a long snake-shaped microchannel, a micropillar array and a vent as schematically illustrated in Fig. 1. Two different inlets for sample and buffer loading connected by a T-junction to a common microchannel were designed for achieving sequential capillary fluid delivery. Furthermore, we designed a highly ordered micropillar array as a capillary pump combined with the microfluidic channel as a flow resistor to generate autonomous and controllable capillary flow [12, 18]. Both the depth of the microfluidic channel and the height of the micropillars were set as 25 µm for easy fabrication. In order to generate steady capillary flow for rapid biomedical detections, the microchannel width was set as 50 µm and the pillar diameter and pitch (pillar centre-centre distance) were set as 5 and 8 µm, respectively, with a high aspect ratio of 5. The snake-shaped microchannel has a total length of around 50 mm (short version), or 120 mm (long version) for comparison. Next, the design considerations will be discussed in detail.

2.1.1. Design of microfluidic channel: To design a device capable of generating steady and robust capillary flow, it is necessary to study the factors which can impact the flow rate of the liquid passing by the microfluidic devices. The flow rate of the liquid in the microchannel with rectangular cross-section can be written as [18]

$$Q = \frac{1}{\eta}\frac{P_{\text{cap}}}{R_F}, \tag{1}$$

where η is the viscosity of the liquid, P_{cap} is the capillary pressure and R_F is the total resistance to flow of the flow path. On the one hand, the capillary pressure in a microchannel with rectangular cross-section has been given as [22]

$$P_{\text{cap}} = \gamma\left(\frac{\cos\theta_t + \cos\theta_b}{d} + \frac{\cos\theta_l + \cos\theta_r}{w}\right), \tag{2}$$

where γ is the surface tension of the liquid, θ_t, θ_b, θ_l, θ_r are the contact angles of the top, bottom, left and right walls, respectively, d is the depth of the channel and w is the width of the channel.

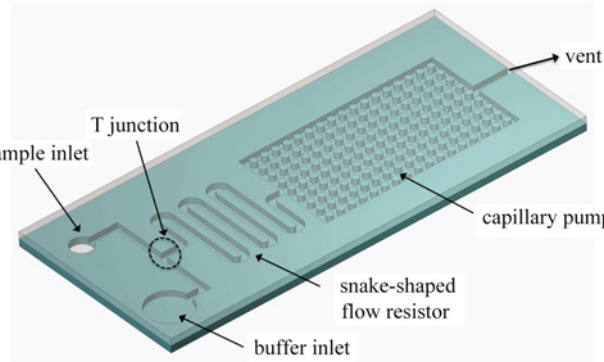

Fig. 1 *Schematic diagram of the Si-based CMD (not in scale)*

The generalised Cassie angle θ^* is defined as the average contact angle [20]. The liquid propagation by capillary force only occurs when Cassie angle is smaller than 90° ($\theta^* < 90°$), and the Cassie angle is given as

$$\cos\theta^* = \frac{d(\cos\theta_l + \cos\theta_r) + w(\cos\theta_t + \cos\theta_b)}{2(d+w)}. \tag{3}$$

For an open microchannel, the contact angle of the top wall (θ_t) is taken to be 180° as the top wall is the air. Meanwhile, as it is difficult to directly measure the contact angle of the bottom and side wall of the microchannels, the contact angles of the bottom and side walls are assumed the same as the flat top surface of the microfluidic device as a proximity for our analysis, meaning $\theta = \theta_b = \theta_l = \theta_r$. Therefore, (2) can be simplified as

$$P_{\text{cap}} = \gamma\left[-\frac{1}{d} + \cos\theta\left(\frac{1}{d} + \frac{2}{w}\right)\right]. \tag{4}$$

Equation (3) can be simplified as

$$\cos\theta^* = \frac{(2d+w)\cos\theta - w}{2(d+w)}. \tag{5}$$

On the other hand, the second important factor, the flow resistance, R_F in microchannel with rectangular cross-section can be approximated by the equation [18]

$$R_F = \left[\frac{1}{12}\left(1 + \frac{5d}{6w}\right)\frac{dwR_H^2}{L}\right]^{-1}, \quad R_H = \frac{dw}{d+w}, \tag{6}$$

when the condition $d < w$ is satisfied, where R_H is the hydraulic radius, L is the length and d and w are the depth and width of the channel, respectively. From (4)–(6), it is clear that the geometric parameters (i.e. d, w, L) and the contact angle of the microchannel are the major factors we should optimise in order to design an optimal microfluidic device. In this Letter, we defined a comprehensive geometric factor G, which is a combination of the different geometric parameters and the contact angle, given as

$$G = \frac{P_{\text{cap}}/\gamma}{R_H/L} = \left[-\frac{1}{d} + \cos\theta\left(\frac{1}{d} + \frac{2}{w}\right)\right] \times \left[\frac{1}{12}dw\left(1 + \frac{5d}{6w}\right)\left(\frac{dw}{d+w}\right)^2\right]. \tag{7}$$

One can see that G is only determined by the depth, the width and the contact angle, and the flow rate can be further simplified as

$$Q = \frac{\gamma}{\eta L}G. \tag{8}$$

From (8), one can see that for a certain fluid (i.e. water), the flow rate is proportional to the geometric factor G. In this study, the depth of 25 µm was chosen according to the reported studies and our microfabrication capability [12, 21]. Different contact angles varying from 0° to 60° were set for our theoretical analysis. Fig. 2 shows the comparative plots of the numerically obtained factor G versus the channel widths and contact angles calculated from (7). For the fixed width, the factor G gradually increases with the decreasing of the contact angle, indicating that a lower contact angle may provide faster flow rate. However, it is usually more difficult to achieve and maintain a very low contact angle for the device due to the contaminations. In reported works, contact angles around 30–45° are usually applied for the capillary purpose [11, 23]. Within this contact angle range, the geometric

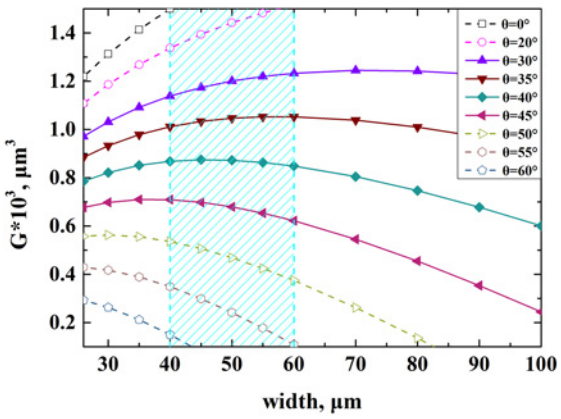

Fig. 2 *Geometric factor G as a function of the width for microchannel with the same depth of 25 μm when the contact angle (θ) varies from 0° to 60°*

factor G first increases with the increase of the channel width, and then decreases with the further increase of the channel width, as shown in Fig. 2. An optimal width range around 40–60 μm was determined, as illustrated in Fig. 2 (in the shadow area). Therefore, in this study the channel width of 50 μm was chosen in order to obtain a stable and relatively high factor G. Once the channel depth (= 25 μm) and the channel width (= 50 μm) were determined, we can calculate the appropriate contact angle of the device according to (5). The obtained results showed that a contact angle smaller than 60° was preferable for our capillary application [20]. In addition, considering the size of the chip and the flow rate appropriate for biosensing applications, two lengths (50 and 120 mm) of the microchannel were designed for comparison.

2.1.2. Design of micropillar array: In this study, a micropillar array was proposed to work as a capillary pump [11, 12, 18]. The volume superficial velocity of the fluid in the micropillar array is determined by the Darcy's law using porous medium approach [24]

$$U = \frac{K}{\mu}\frac{\mathrm{d}P}{\mathrm{d}x}, \tag{9}$$

where μ is the viscosity of the liquid, K is the permeability and P is the capillary pressure of the array. Therefore, the micropillar array with high permeability (K) and high capillary pressure (P) is preferred as a capillary pump. According to (9), different permeability leads to different capillary performance, determined by the porosity or the solid fraction of the array. For a hexagonal pillar array we proposed in this study, the porosity (ε) and the solid fraction (f) are, respectively, written as

$$\varepsilon = 1 - \frac{\sqrt{3}\pi}{6}\left(\frac{D}{p}\right)^2, \tag{10}$$

$$f = 1 - \varepsilon = \frac{\sqrt{3}\pi}{6}\left(\frac{D}{p}\right)^2, \tag{11}$$

where D is the diameter of micropillar, and p is the pitch (pillar centre-centre distance). To simplify the calculation, the permeability K can be expressed by simplifying a flat meniscus at the liquid/air interface as [25]

$$K = K_0\left[1 - \frac{\mathrm{e}^{2h\sqrt{\varepsilon/K_0}} - 1}{h\sqrt{\varepsilon/K_0}\left(\mathrm{e}^{2h\sqrt{\varepsilon/K_0}} + 1\right)}\right] \tag{12}$$

where K_0 is the permeability of planner pillar array and h is the height of the pillar. The permeability of planner pillar array with high and low porosity has been studied, respectively, and K_0 has been modelled as the following two expressions [26]:

$$K_0 = \frac{p^2}{4\pi}\ln\left(f^{-0.5} - 0.745 + f - 0.25f^2\right), \quad \text{when } f < 0.4 \tag{13}$$

$$K_0 = \frac{4\sqrt{2}p^2}{27\pi}\left(1 - \sqrt{\frac{2\sqrt{3}f}{\pi}}\right)^{5/2}, \quad \text{when } f > 0.65 \tag{14}$$

The experimentally obtained K_0 matches well with the expressions (13) and (14) when f is satisfied with the conditions above, and the real K_0 is close to the result from the expression (13) when f is between 0.4 and 0.65 [26]. Considering the fabrication complexity, the pillar height of 25 μm (the same height as the depth of the microchannel) was designed. Meanwhile, the micropillar diameter of 5 μm was chosen for a high aspect ratio of 5. Using the expressions (10)–(14), the relationship between the permeability and the solid fraction can be calculated, and the result is shown in Fig. 3, where the permeability decreases with increasing solid fraction. However, unlike permeability, the capillary pressure (P) of the micropillar array increases with increasing solid fraction from simulations and experiments [17]. In this study, a compromise between high capillary pressure and high permeability was made, and a solid fraction of 0.354 with pitch of 8 μm was chosen for our capillary microfluidic device design.

2.2. Device fabrication: The device is fabricated using the standard lithographic technique in combination with deep Si etch technique [27]. In brief, the device pattern was first defined on 500 nm-thick positive photoresist spun on a 400 nm SiO_2-covered Si wafer using UV lithography. Next, the structure pattern was transferred to the SiO_2 layer underneath. The inlets, the microchannel and the micropillar array were simultaneously etched on the Si substrate by using the Bosch etching process using the SiO_2 pattern as a hard mask [27]. The microstructure of the device was characterised using scanning electron microscopy (SEM).

2.3. Surface modification: As discussed above, the surface hydrophobicity of microfluidic device plays a critical role. In this study, in order to achieve a low contact angle of the device, different surface hydrophilisation modification techniques were studied and compared on our devices, including oxygen plasma treatment, SiO_2 coating and SAM deposition of azide silane. Hereto, the prepared Si CMDs were pre-treated by oxygen plasma in a home-made instrument (pressure = 0.263 Torr, power = 100 W) [19]. Then, a 50 nm SiO_2 layer was thermally grown on one set of the CMDs [28]. To have a SAM coating

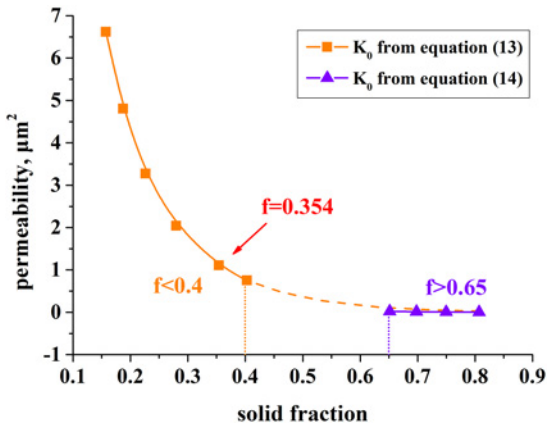

Fig. 3 *Permeability (K) as a function of solid fraction for micropillar arrays with the same diameter and height. The values of K_0 in the orange line and the violet line are calculated from (13) and (14), respectively*

doi: 10.1049/mnl.2018.5120

on the device surface, some of SiO_2-covered CMDs were further deposited on a layer of azide silane using a similar protocol as described elsewhere [19, 29]. In brief, after the aforementioned oxygen plasma cleaning, the SiO_2-covered devices were immersed in a solution containing 2% (v/v) 11-azidoundecyltriethoxysilane dissolved in a mixture of 95:5 ethanol/water (v/v) overnight for azide silane deposition. Thereafter, the devices were rinsed thoroughly with ethanol, dried in a N_2 stream. The silane cross-linking was promoted in an oven at 110°C for 10 min. The surface modified devices were stored in a dark box in air until further use. Each step mentioned above in surface modification was observed in contact angle as an evident change. Water contact angle measurements were carried out at room temperature using a contact angle analyser (Dataphysics Instruments, Germany). At least ten data points on three different samples were repeated for each condition.

2.4. Microfluidic experiments: To assess the capillary capability of the fabricated CMDs, liquid filling time experiments were carried out as proposed by other researchers [11, 30]. In addition, to demonstrate the capability of sequential capillary flow generation for multi-step biological detection, the deionised water stained with 100 nM Cy3 dye and the deionised water were added to the CMDs from the buffer inlet and the sample inlet in succession. The capillary flow generation and propagation inside the CMDs were monitored by a bright-field microscope equipped with a video recorder. The propagation distance and the average flow rate inside the microchannel and inside the micropillar array were calculated based on the recorded video [11, 30].

3. Results and discussion

3.1. Device characterisation: Fig. 4 shows the photograph of the fabricated device and the SEM images of the microchannel and the micropillars before surface modification. Fig. 4*a* shows the Si chip of 32 mm × 30 mm with two independent CMDs consisting of different channel length for the flow resistor. The device has a total volume of ~30 µl. As seen in Fig. 4*b*, the snaked-shaped microchannel has a channel width of around 50 µm and a depth of around 25 µm with vertical channel walls and around corners at the inflection points, indicating the miniaturisation of possible dead volume [12]. Figs. 4*c* and *d* show the hexagonal array of cylindrical Si micropillars with diameter (D) of 5 µm, pitch (p) of 8 µm and height (h) of 25 µm, which gives a high aspect ratio of 5.

3.2. Surface modification characterisation: Since wetting of the surface is one of the key points for liquid propagation on the device, it is crucial to have a well-controlled device surface property. To obtain a robust capillary flow in the CMDs, the contact angle is better smaller than 60° as we calculated before. Furthermore, it is reported that a contact angle in the range of 30–45° is preferred [11, 23]. As it is difficult to directly measure the contact angle inside the microchannel and microstructures, the contact angles of the blank areas were measured on the top surface of the device to evaluate the contact angle variation trends after three different surface modification procedures [7, 11]. The native Si device has a contact angle of around 70° larger than 60°. Thus, the surface has to be modified in order to generate a capillary flow. Fig. 5 shows the resultant contact angles after various surface modifications and their evolutions after exposure in air for different time. For the un-coated Si device, after the oxygen plasma treatment which is usually used as a cleaning procedure for various surface, the device is transformed into a very hydrophilic surface with a contact angle below 10°, but its contact angle increases rapidly to around 20° within an hour, further increases to around 51° in a week, and finally reaches its native contact angle of around 70° after 3 months partially attributed to air contamination. This observation agrees very well with previous studies [11, 31]. For the SiO_2 coated device, the contact angle gradually increased in the first 2 months and finally stabilised at around 38°. However, unlike the aforementioned two methods with great variation of the contact angles in the 3-month evaluation period, for the

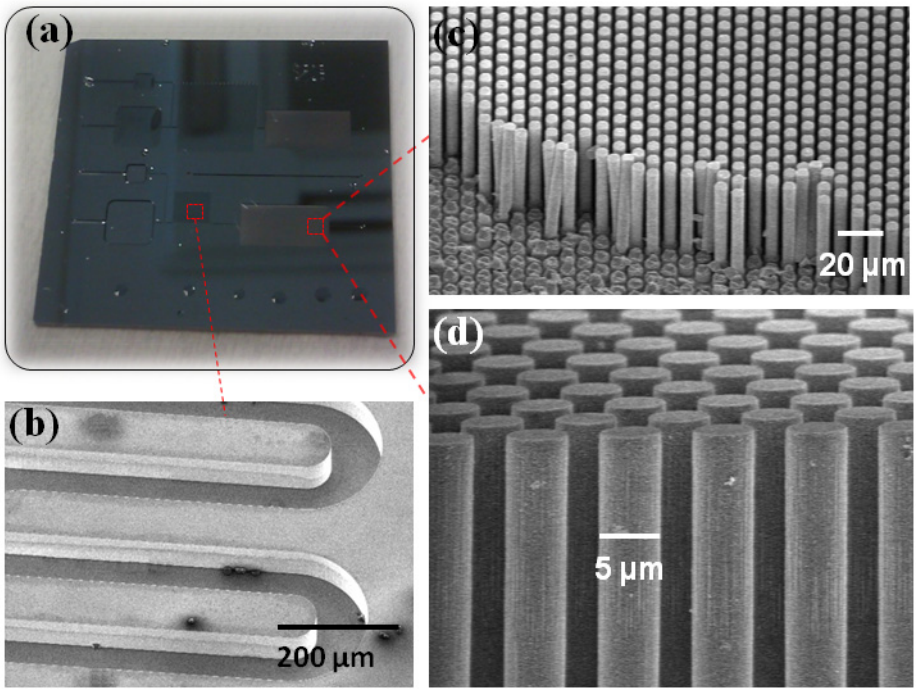

Fig. 4 *Fabricated CMD*
a Photograph of the fabricated 32 mm × 30 mm CMD
b SEM image of the snake-shaped microchannels
c SEM image of the micropillar array with 5 µm in diameter and 25 µm in height
d Cross-sectional SEM image of the micropillar array

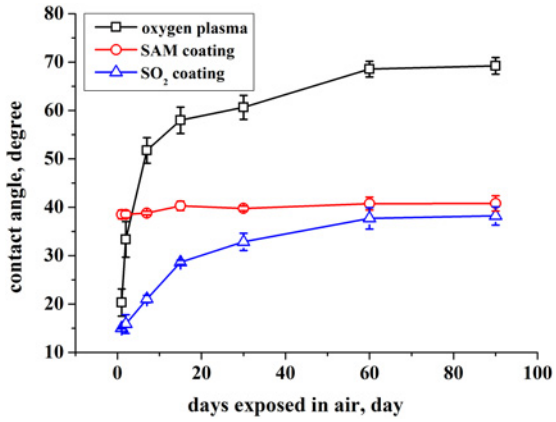

Fig. 5 *Contact angle variations of the CMDs after various surface modifications and their evolutions as a function of time exposed in air*

SAM-coated device, the contact angle slightly increases to 40°, and can keep stable for at least 3 months, indicating a very good stability of the SAM deposition on the device. Therefore, the SAM deposition on the device provides a good and long-term method for device surface modification. This result is consistent with the reported azide silane-modified surfaces on glass or polymer substrates [23, 32]. Stable and hydrophilic device surface ensures the flexibility of the capillary fluidic control.

3.3. Microfluidic characterisation: In this study, the various functional elements, such as the microchannel, the micropillar array and two separated inlets are directly built into a single CMD, which allows autonomous, sequential capillary flow generation and capillary pumping. First, the autonomous capillary flow inside the snake-shaped microchannel was evaluated using the SAM-coated CMDs. Fig. 6 shows the water fluid propagation distance inside the snake-shaped microchannel as a function of time by adding 20 µl aliquot of deionised water into the buffer inlet. As shown in Fig. 6, The CMD has a snake-shaped microchannel with a total length of either 120 mm (upper device in Fig. 4*a*) or 50 mm (down device in Fig. 4*a*). It takes 65 s to penetrate into the entire 120 mm-long flow resistor with an overall average flow rate of around 1.85 mm/s, which is in the range of suggested flow rate for immunoassay detection

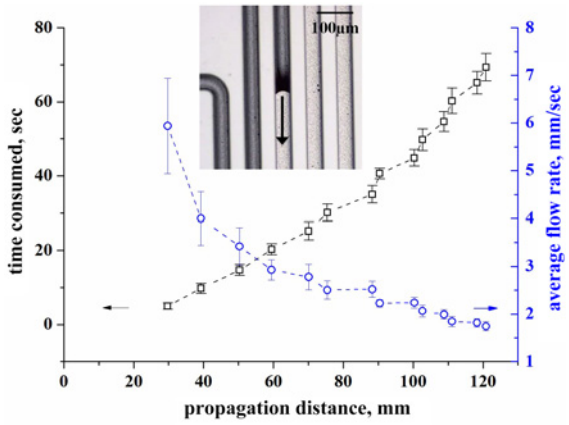

Fig. 6 *Liquid propagation in the microchannel of the device. The black curve indicates the relationship between the propagation distance and the time consumed, and the blue curve indicates the relationship between the overall average capillary flow rate and the propagation distance. Error bars represent the deviations of at least three independent measurements on each condition. The inset shows an instant during liquid propagation experiment*

(0.2–2 mm/s) in microfluidic devices [11]. However for the short microchannel, it only takes around 15 s to accomplish the penetration with an overall average flow rate of 3.3 mm/s. In this study, the flow resistor with an appropriate length, i.e. 120 mm, allows an appropriate capillary flow rate at the end of the microchannel, which may be beneficial for the biosensing application as it can prolong the bio-reaction time [11, 12].

Second, the capability of sequential capillary flow generation was demonstrated on the device with deionised water and deionised water stained with 100 nM Cy3 dye as it is important for the multi-step bioassay detection. As shown in Figs. 7a_1 and a_2, when 1 µl of Cy3 stained HB is added into the device via the sample inlet, the generated capillary flow passes over the T-junction and penetrates along the snake-shaped microchannel with a gradually decreased flow rate (Fig. 6) until the 1 µl aliquot in the sample inlet is completely exhausted (Fig. 7a_3). Afterwards, a larger volume of deionised water (20 µl) is added via the buffer inlet, as shown in Fig. 7a_4. Since there is only one common outlet, the unstained capillary flow generated by capillarity also follows the stained capillary flow inside the microchannel, passes over the T-junction and penetrates sequentially inside the snake-shaped channel. The entire procedure can also be observed from the recorded video with a bright-field microscope, as shown in Figs. 7b_1–b_4. From both the fluorescent observation and bright-field observation, there is no air bubble entrapped inside the microchannels due to the open microchannel [9, 11]. In addition, the unstained capillary flow and stained capillary flow sequentially propagate along the microchannel with a minimal mixing or crosstalk, which may be attributed to the low Reynolds number of the laminar flow inside a 50 µm-wide channel [14]. This type of precise control over fluid distribution rates and orders may be very useful particularly for the complex bio-assays that require multiple steps and multiple reagents [14].

To evaluate the pumping ability of the micropillar array, one-dimensional liquid propagation experiment was carried out with a dummy testing device which has a micropillar array of 50 mm long and 8 mm wide, as shown in Fig. 8*a* [30]. The micropillars on the dummy device are exactly the same as the CMD, and are surface modified as described above using the azide-silane SAM protocol. The dummy device was positioned vertically over a beaker filled with deionised water and was partially submerged into the liquid. The liquid meniscus rise along the micropillar array was recorded and the wicking capability was assessed. Fig. 8*b* shows the resultant water propagation distance as a function of the propagation time, and the corresponding overall average flow rate. As seen, the entire micropillar array of 50 mm was completely penetrated with water within 2 min, indicating that the 8 mm × 5 mm capillary pump area designed on the CMD was appropriate. Furthermore, when evaluating the average capillary flow rate along the propagation direction, one could see that the

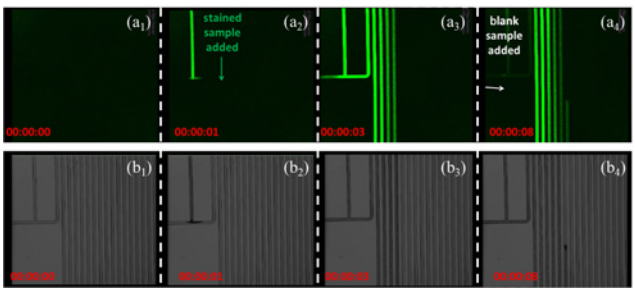

Fig. 7 *Autonomous and sequential capillary flow generation and propagation in the microchannel*
a_1–a_4 Time-lapse fluorescent images during capillary flow propagating
b_1–b_4 Time-lapse bright-field images of the corresponding capillary flow propagating

doi: 10.1049/mnl.2018.5120

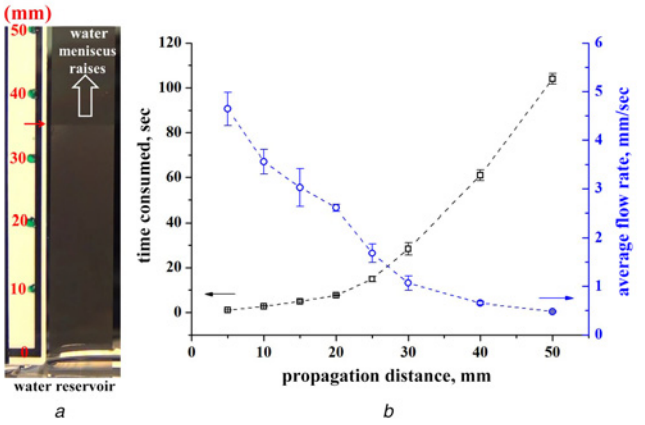

Fig. 8 *Liquid propagation in the micropillar array of the device*
a Photograph of an instant during liquid propagation experiment in the micropillar array. The red arrow indicates the liquid front and the hollow arrow indicates the propagation direction
b Black curve indicates the relationship between propagation distance and the time consumed, and blue curve indicates the relationship between the average capillary flow rate and the propagation distance. Error bars represent the deviations of at least three independent measurements on each condition

flow rate was also gradually decreased, which was consistent with the observation in the microchannel and agrees well with previous reports [11, 30].

4. Conclusion: In this work, a compact open Si-based capillary microfluidic device was designed and fabricated. The hydrophilic surface modification of the device was completed by coating a thin layer of SAM. The surface modified device achieved a contact angle of around 40° stabilised for at least 90 days. The device utilised the microchannel in combination with the micropillar array with high aspect ratio of 5 for controllable capillary fluid delivery. In addition, sequential capillary flow generation was demonstrated without bubble generation and clogging due to the open device we designed. Therefore, the proposed Si-based capillary microfluidic device makes possible for complex and multi-step biological assays and shows a great potential for the POCT applications.

5. Acknowledgments: The authors acknowledge the financial support of National Natural Science Foundation of China (grant nos. 61571437, 61774167), National Key Research and Development Plan of China (grant no. 2016YFC0900200) and Beijing Natural Science Foundation (grant no. 4182072).

6 References

[1] Yager P., Edwards T., Fu E., *ET AL.*: 'Microfluidic diagnostic technologies for global public health', *Nature*, 2006, **442**, (7101), pp. 412–418
[2] Gervais L., de Rooij N., Delamarche E.: 'Microfluidic chips for point-of-care immunodiagnostics', *Adv. Mater.*, 2011, **23**, (24), pp. H151–H176
[3] Laser D.J., Santiago J.G.: 'A review of micropumps', *J. Micromech. Microeng.*, 2004, **14**, (6), pp. R35–R64
[4] Su W., Gao X., Jiang L., *ET AL.*: 'Microfluidic platform towards point-of-care diagnostics in infectious diseases', *J. Chromatogr. A*, 2015, **1377**, pp. 13–26
[5] Delamarche E., Juncker D., Schmid H.: 'Microfluidics for processing surfaces and miniaturizing biological assays', *Adv. Mater.*, 2005, **17**, (24), pp. 2911–2933
[6] Mastichiadis C., Niotis A.E., Petrou P.S., *ET AL.*: 'Capillary-based immunoassays, immunosensors and DNA sensors – steps towards integration and multi-analysis', *TRAC Trends Anal. Chem.*, 2008, **27**, (9), pp. 771–784
[7] Huang C., Bonroy K., Reekman G., *ET AL.*: 'An on-chip localized surface plasmon resonance-based biosensor for label-free monitoring of antigen–antibody reaction', *Microelectron. Eng.*, 2009, **86**, (12), pp. 2437–2441
[8] Martinez A.W., Phillips S.T., Whitesides G.M., *ET AL.*: 'Diagnostics for the developing world: microfluidic paper-based analytical devices', *Anal. Chem.*, 2010, **82**, (1), pp. 3–10
[9] Posthuma-Trumpie G.A., Korf J., van Amerongen A.: 'Lateral flow (immuno) assay: its strengths, weaknesses, opportunities and threats. A literature survey', *Anal. Bioanal. Chem.*, 2009, **393**, (2), pp. 569–582
[10] Fobel R., Kirby A.E., Ng A.H., *ET AL.*: 'Paper microfluidics goes digital', *Adv. Mater.*, 2014, **26**, (18), pp. 2838–2843
[11] Jonsson C., Aronsson M., Rundstrom G., *ET AL.*: 'Silane-dextran chemistry on lateral flow polymer chips for immunoassays', *Lab Chip*, 2008, **8**, (7), pp. 1191–1197
[12] Gervais L., Delamarche E.: 'Toward one-step point-of-care immunodiagnostics using capillary-driven microfluidics and PDMS substrates', *Lab Chip*, 2009, **9**, (23), pp. 3330–3337
[13] Lillehoj P.B., Wei F., Ho C.M.: 'A self-pumping lab-on-a-chip for rapid detection of botulinum toxin', *Lab Chip*, 2010, **10**, (17), pp. 2265–2270
[14] Novo P., Volpetti F., Chu V., *ET AL.*: 'Control of sequential fluid delivery in a fully autonomous capillary microfluidic device', *Lab Chip*, 2013, **13**, (4), pp. 641–645
[15] Taher A., Jones B., Fiorini P., *ET AL.*: 'A valveless capillary mixing system using a novel approach for passive flow control', *Microfluid. Nanofluid.*, 2017, **21**, (8), pp. 143–153
[16] Sainiemi L., Nissila T., Jokinen V., *ET AL.*: 'Fabrication and fluidic characterization of silicon micropillar array electrospray ionization chip', *Sens. Actuators, B*, 2008, **132**, (2), pp. 380–387
[17] Youngsuk N., Sharratt S., Byon C., *ET AL.*: 'Fabrication and characterization of the capillary performance of superhydrophilic Cu micropost arrays', *J. Microelectromech. Syst.*, 2010, **19**, (3), pp. 581–588
[18] Zimmermann M., Schmid H., Hunziker P., *ET AL.*: 'Capillary pumps for autonomous capillary systems', *Lab Chip*, 2007, **7**, (1), pp. 119–125
[19] Liang L., Astruc D.: 'The copper(I)-catalyzed alkyne-azide cycloaddition (CuAAC) 'click' reaction and its applications. An overview', *Coord. Chem. Rev.*, 2011, **255**, (23–24), pp. 2933–2945
[20] Berthier J., Brakke K.A., Berthier E.: 'A general condition for spontaneous capillary flow in uniform cross-section microchannels', *Microfluid. Nanofluid.*, 2013, **16**, (4), pp. 779–785
[21] Yang D., Krasowska M., Priest C., *ET AL.*: 'Dynamics of capillary-driven flow in open microchannels', *J. Phys. Chem. C*, 2011, **115**, (38), pp. 18761–18769
[22] Delamarche E., Bernard A., Schmid H., *ET AL.*: 'Microfluidic networks for chemical patterning of substrates: design and application to bioassays', *J. Am. Chem. Soc.*, 1998, **120**, (3), pp. 500–508
[23] Dudek M.M., Gandhiraman R.P., Volcke C., *ET AL.*: 'Evaluation of a range of surface modifications for the enhancement of lateral flow assays on cyclic polyolefin micropillar devices', *Plasma Proceses Polym.*, 2009, **6**, (10), pp. 620–630
[24] Kaviany M.: 'Principles of heat transfer in porous media' (Springer, New York, 1995)
[25] Byon C., Kim S.J.: 'The effect of meniscus on the permeability of micro-post arrays', *J. Micromech. Microeng.*, 2011, **21**, (11), p. 115011
[26] Sangani A.S., Acrivos A.: 'Slow flow past periodic arrays of cylinders with application to heat transfer', *Int. J. Multiph. Flow*, 1982, **8**, (3), pp. 193–206
[27] Majeed B., Jones B., Tezcan D.S., *ET AL.*: 'Silicon based system for single-nucleotide-polymorphism detection: chip fabrication and thermal characterization of polymerase chain reaction microchamber', *Jpn. J. Appl. Phys.*, 2012, **51**, p. 04DL01
[28] Ryken J., Li J., Steylaerts T., *ET AL.*: 'Biosensing with SiO_2-covered SPR substrates in a commercial SPR-tool', *Sens. Actuators, B*, 2014, **200**, pp. 167–172
[29] Vranken C., Deen J., Dirix L., *ET AL.*: 'Super-resolution optical DNA mapping via DNA methyltransferase-directed click chemistry', *Nucleic Acids Res.*, 2014, **42**, (7), p. e50
[30] Xiao R., Enright R., Wang E.N.: 'Prediction and optimization of liquid propagation in micropillar arrays', *Langmuir*, 2010, **26**, (19), pp. 15070–15075
[31] Huang C., Bonroy K., Reekmans G., *ET AL.*: 'Localized surface plasmon resonance biosensor integrated with microfluidic chip', *Biomed. Microdevices*, 2009, **11**, (4), pp. 893–901
[32] Prakash S., Karacor M.B.: 'Characterizing stability of 'click' modified glass surfaces to common microfabrication conditions and aqueous electrolyte solutions', *Nanoscale*, 2011, **3**, (8), pp. 3309–3315